Supplementary information
Unconventional spin relaxation involving localized vibrational modes in Ho single-atom magnets

F. Donati,[1,2,3] S. Rusponi,[2] S. Stepanow,[4] L. Persichetti,[4,5] A. Singha,[1,2,3]
D. M. Juraschek,[4,6] C. Wäckerlin,[2,7] R. Baltic,[2] M. Pivetta,[2] K. Diller,[2] C. Nistor,[4]
J. Dreiser,[8] K. Kummer,[9] E. Velez-Fort,[9] N. Spaldin,[4] H. Brune,[2] and P. Gambardella[4]

[1] *Center for Quantum Nanoscience, Institute for Basic Science (IBS), 03760 Seoul, Republic of Korea*
[2] *Institute of Physics, École Polytechnique Fédérale de Lausanne (EPFL), Station 3, CH-1015 Lausanne, Switzerland*
[3] *Department of Physics, Ewha Womans University, Seoul 03760, Republic of Korea*
[4] *Department of Materials, ETH Zurich, Hönggerbergring 64, CH-8093 Zurich, Switzerland*
[5] *Department of Sciences, Roma Tre University, I-00146, Roma, Italy*
[6] *Harvard John A. Paulson School of Engineering and Applied Sciences, Harvard University, Cambridge, MA 02138, USA*
[7] *Institute of Physics of the Czech Academy of Sciences, Cukrovarnická 10, 16200 Prague 6, Czech Republic*
[8] *Swiss Light Source (SLS), Paul Scherrer Institute (PSI), CH-5232 Villigen PSI, Switzerland*
[9] *European Synchrotron Radiation Facility (ESRF), F-38043 Grenoble, France*

I. EXPERIMENTAL DETAILS

The XAS and XMCD measurements were performed at the EPFL/PSI X-Treme beamline at the Swiss Light Source [1] and at the ID32 beamline at the European Synchrotron Radiation Facility [2]. Both endstations are equipped with an ultra-high vacuum chamber for sample preparation (base pressure 3×10^{-10} mbar) and an Omicron variable-temperature scanning tunnelling microscope (VT-STM). All measurements were performed in normal incidence geometry with circularly polarized light in the total electron yield (TEY) mode at sample temperatures down to $T = 2.5$ K, and in external magnetic fields up to $B = 6.8$ T parallel to the x-ray beam. In order to isolate the contribution of the Ho atoms from the background signal, spectra of bare MgO/Ag(100) over the Ho M_5 edge are recorded prior to Ho deposition and subtracted from the final spectra.

Each point in the relaxation plot of Fig. 1 of the main text is obtained by acquiring the XAS signal for the two circular polarizations at the maximum of the XMCD edge as a function of time after saturating the ensemble to the maximum positive or negative value of the magnetic field. During the sweep of the magnetic field from the saturating to the measurement value, the beam shutter was kept close to prevent undesired photon-induced relaxation. In this way, the ensemble is largely preserved in its saturated state until the beginning of the measurement. Also note that even at high temperature we can mostly neglect spontaneous relaxation occurring prior to reach the field of measurement. In fact, these processes have been shown to be relevant only for fields below $B = 0.3$ T. The time required to sweep across this low field region and reach the target field of $B = 0.01$ T is about 10 s, a time that is not significantly relevant compared the values of τ observed in this work. Therefore, these undesired relaxation occurring prior to the measurement's start have limited impact on the experiment itself.

The XAS from the two opposite polarizations was normalized to the corresponding pre-edge signal measured 7 eV below the XMCD peak, also acquired in the same sequence, to compensate for any spurious variation of the beam intensity during the acquisition. In order to minimise the influence of the photon beam on the lifetime of the magnetic atoms [3], all the measurements were performed at the smallest photon flux ensuring a sufficient signal to noise ratio, previously shown to be $\phi_0 = 0.14 \times 10^{-2}$ nm^{-2} s^{-1} [4].

Single crystals of Ag(100) were prepared with repeated cycles of sputtering and subsequent annealing at 773 K. Films of MgO with thickness between 4 and 6 monolayers (MLs) were grown by thermal evaporation of Mg in O_2 partial pressure of 1×10^{-6} mbar, with the substrate kept at 623 K and a Mg flux yielding a growth rate of about 0.2 ML/min. One monolayer is defined as one MgO(100) unit cell per Ag(100) substrate atom. The calibration of the MgO thickness was obtained from comparison of STM images and XAS spectra at the Mg K edge of samples covered with close to half a monolayer of MgO. We then estimated the thickness of the MgO films assuming a linear relation between the amplitude of the Mg K edge and the amount of deposited MgO. The samples were transferred to the measurement position without breaking the vacuum. Holmium atoms were deposited from a thoroughly degassed rod (purity 99.95 %) on the substrate held at less than 10 K and in a base pressure of 4×10^{-11} mbar. To minimize the presence of clusters in the ensemble, we limited the Ho coverage below 0.015 ML in all the experiments, where again 1 ML is defined as one Ho atom per Ag(100) substrate atom. For the MgO thicknesses and substrate temperatures

applied here, the Ho atoms occupy with more than 90 % probability the O on-top site [5]. The amount of Ho on the surface is calibrated by comparison with former experiments [4, 6, 7].

II. ESTIMATION OF THE EFFECTIVE ENERGY BARRIER USING ARRHENIUS FUNCTION

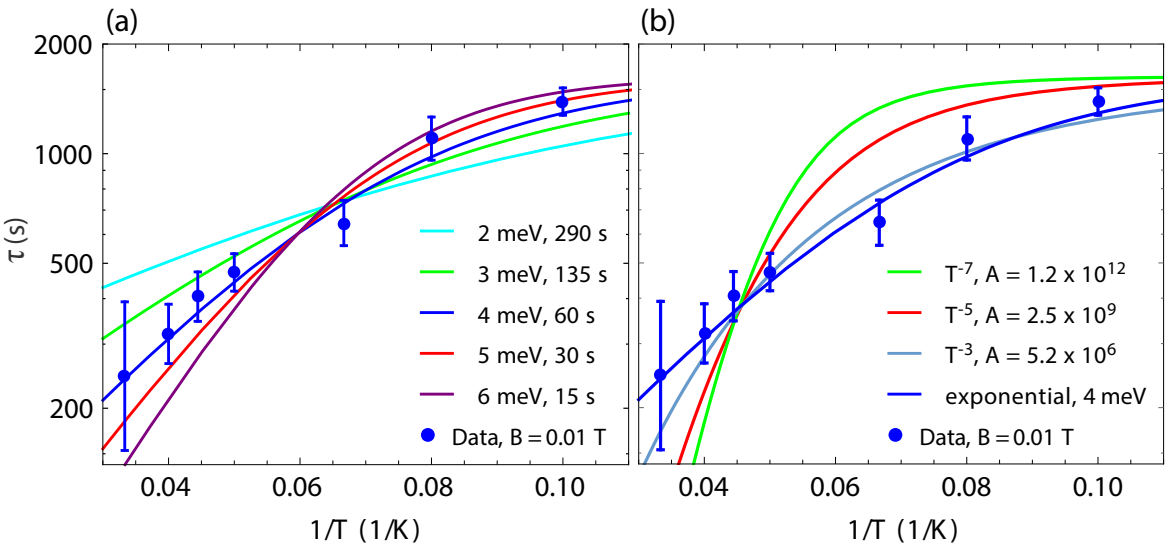

Figure S1. (a) Magnetic lifetime, τ, versus temperature for $B = 0.01$ T (blue dots). Solid lines are plots of $\tau(T)$ calculated using Eq. (S1) for different values U_{eff} and τ_0 ($\tau_\nu = 1630$ s). (b) Comparison between plots using Eq. S2 (T^{-n}) with various values of n and best fit using Eq. (S1) (exponential, blue solid line).

As discussed in the main text, the temperature dependence of τ at $B = 0.01$ T can be fit by

$$\tau_{\text{Arr}}^{-1} = \tau_\nu^{-1} + \left[\tau_0 \exp\left(U_{\text{eff}}/k_{\text{B}}T\right)\right]^{-1}, \tag{S1}$$

where $\tau_\nu = 1630$ s is the photon-limited lifetime due to the secondary electrons [4], and the exponential term describes a thermally-activated relaxation with an effective barrier U_{eff} and a prefactor τ_0. As shown in Fig. S1(a), best fit to the data gives $U_{\text{eff}} = 4 \pm 1$ meV and $\tau_0 = 60 \pm 30$ s.

In order to further evince the origin of this relaxation process, we consider the expected rate obtained from Raman-processes activated by the continuum of delocalized substrate phonons. In this case, one finds a relaxation rate that follows a power law [8, 9] with characteristic exponent depending on the spin multiplicity and dimensionality of the phonon modes. Including the photon-limited relaxation, the magnetic lifetime reads

$$\tau_{Ram}(T)^{-1} = \tau_\nu^{-1} + \left[AT^{-n}\right]^{-1}, \tag{S2}$$

with A being a rescaling prefactor. For non-Kramers ions, the characteristic exponent takes values of $n = 7$ or 5 when phonon modes with 3D or 2D dispersion relations, respectively, are involved. Best fits using these two power laws cannot reproduce the low field data, see Fig. S1(b). Only lowering the exponent to $n = 3$ produces a fair fit, although less accurate than the best fit using Eq. (S1).

The required low value of the characteristic exponent suggests that the coupling to delocalized phonons cannot account for the observed spin relaxation. In the literature, non-conventional values of the characteristic exponent are often found in molecules with very large magnetic anistropy [10, 11] and attributed to the presence of localized modes with sharp resonances in the DOS. As shown in Sec. IV, a proper description of these local modes in surface-adsorbed atoms leads to a characteristic exponential temperature law. We finally note that, even if a power law with low exponent could provide an approximate fit to the low field data, processes that involves a monotonic phonon DOS are expected to provide a relaxation rate that increases with the external field, see Sec. IV, hence they cannot account for the observed behavior at high field.

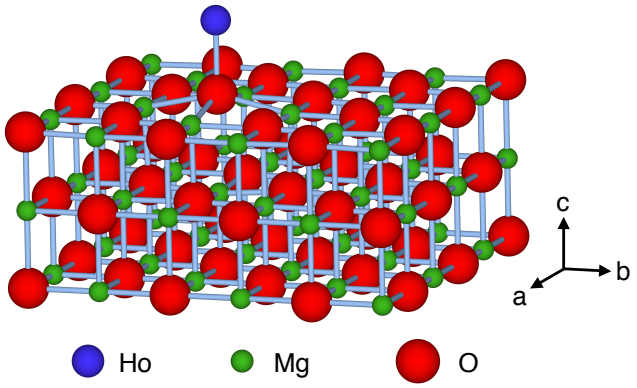

Figure S2. Unit cell of one Ho atom on three monolayers of MgO with the bottom layer fixed to the lattice spacing of Ag(100) at 289 pm. The oxygen lying below the Ho is protruded from the surface by 47±2 pm.

III. COMPUTATIONAL DETAILS

We calculated the vibrational eigenfrequencies and eigenvectors of a Ho atom on three monolayers of MgO from first-principles using the density functional theory (DFT) formalism as implemented in the Vienna ab-initio simulation package (VASP) [12, 13] and the frozen-phonon method as implemented in the phonopy package [14]. We used a 109-atom unit cell with Ho located above a surface oxygen and topped by 16 Å of vacuum, and we fixed the bottom MgO layer to the lattice spacing of Ag(100) at 289 pm. Since MgO was shown to act as an efficient filter for the phonon modes of a substrate [4], we do not take the Ag substrate into account in this calculation. We used the default VASP PAW pseudopotentials and converged the Hellmann-Feynman forces to 10^{-5} eV/Å using a plane-wave energy cut-off of 750 eV and a 2×2×1 k-point mesh to sample the Brillouin zone. For the exchange-correlation functional we chose the PBEsol form of the generalized gradient approximation (GGA) [15, 16]. Our fully relaxed structure with a MgO surface lattice spacing of 289 pm fits reasonably well to the experimental values [4]. The Ho atom is elevated 251±1 pm above the slightly buckled MgO surface and 204 pm above the protruded oxygen. An illustration of the unit cell is shown in Fig. S2. Crystal structures were visualized using the VESTA package [17].

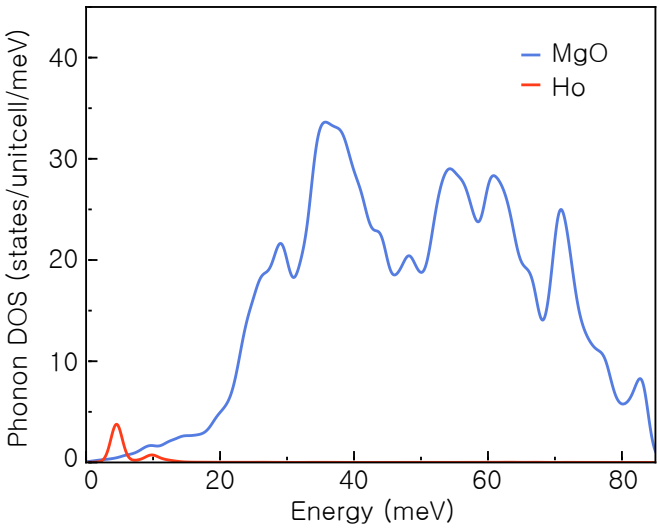

Figure S3. Calculated phonon DOS projected onto the contributions of the Ho atom and the MgO slab, respectively.

Frozen-phonon calculations reveal two degenerate modes at the Brillouin zone center involving mainly the motion of the Ho atom parallel to the surface at 4.7 meV and perpendicular to the surface at 8.6 meV. These vibrations distinctively show up in the phonon density of states as two peaks in the low-frequency regime, as is shown in Fig. 4a of the main text and in Fig. S3. Vibrational modes involving mainly the ions of the MgO slab lie at higher frequencies above roughly 20 meV. The eigenvectors of the Ho atom and the below lying oxygen are shown schematically in

Fig. 4b of the main text. Our calculation of the localized vibrational modes yields two degenerate in-plane modes and one out-of-plane mode in accordance with the P4mm symmetry of the Ho adsorption site on top of oxygen, and in contrast to previous calculations, in which the symmetry was not maintained [4].

The calculated phonon DOS supports the assumptions of the two-phonon relaxation model developed in this work, with the local vibrations providing the largest contribution. The main arguments supporting the weak coupling to the MgO delocalized phonon modes are the following. Firstly, at low energy the phonon DOS of the acoustic modes is quite low. In addition, the long range waves only provide very small relative displacement on the atomic scale, which in turns limits the effect on the local change of the magnetic anisotropy. Secondly, although optical phonon modes could provide the required perturbation to the local environment [18], the high energy required to activate these modes in MgO ($50 - 80$ meV) strongly limits their contribution in the temperature range of our experiments. Consequently, the most effective contribution to the spin-reversal has to stem from the local vibrations, as these modes provide large displacement of the Ho atoms at an energy that can be activated at low temperature, as shown in Fig. S3.

IV. RAMAN MODEL OF MAGNETIC RELAXATION

The long magnetic lifetimes measured at low fields and the large magnetic remanence observed in hysteresis loops [4] suggests that, for Ho atoms, quantum tunneling of the magnetization is slower than the photon-induced relaxation. Similarly, the absence of a characteristic decrease of the spin lifetime with increasing magnetic field suggests that direct processes are not effectively contributing to the spin relaxation up to the longest time scale available in our experiments (thousands of seconds). As discussed in a previous work [19], two alternative level schemes with either $J_z = 7$ or 8 ground state can possibly explain the available experimental data [4, 19, 20]. In a more recent paper [21], it was shown that the behavior of Ho atoms at small magnetic fields is compatible with a $J_z = 8$ ground state where the hyperfine interaction creates several avoided level crossings. In both scenarios, due to the C_{4v} symmetry of the adsorption site, the ground state doublet is not a pure state of the operator $\hat{J}_z$ and the admixture of states with lower axial character enables transitions across the anisotropy barrier. Assuming the eigenstates of the system to be product states between spin and phonon states [22], spin reversal can occur through $\Delta m = \pm 2$ or $\Delta m = 0$ transitions for a $J_z = 7$ or 8 ground state, respectively. In both cases, realizing these transitions requires the transfer of angular momentum of two quanta carrying a momentum $\Delta m = \pm 1$ [22]. Supported by these arguments, and in the absence of clear signatures related to spin reversal driven by quantum tunnelling of the magnetization and direct processes, we develop a model for the magnetic lifetime of Ho atoms that only includes two-phonon Raman processes and photon-induced relaxation.

Specifically, we include the contribution of spatially localized vibrations following the approach of D.L. Mills [23]. These vibrational modes are modeled with gaussian peaks:

$$D_{\mathrm{v}}(\omega - \omega_{\mathrm{v}}) = \frac{\exp\left[\frac{(\omega-\omega_{\mathrm{v}})^2}{2\sigma_\omega^2}\right]}{\hbar\sqrt{2\pi}\sigma_\omega} \tag{S3}$$

at the frequencies $\omega_{\mathrm{v}} = \omega_{\parallel} = E_{\parallel}/\hbar = 4.7$ meV$/\hbar$ and $\omega_{\mathrm{v}} = \omega_{\perp} = E_{\perp}/\hbar = 8.6$ meV$/\hbar$ as calculated by DFT. The broadening σ_ω is related to the full-width-half-maximum (FWHM) of the gaussian peak by $\Delta\omega = \Delta E/\hbar = 2\sqrt{2\ln 2}\sigma_\omega$. It is a free parameter of the model and is determined from the fit of the experimental data. For the model described in the main text, we only include the projected phonon DOS on the Ho atoms:

$$D_{\mathrm{Ho}}(\omega) = 2D_{\mathrm{v}}(\omega - \omega_{\parallel}) + 0.4D_{\mathrm{v}}(\omega - \omega_{\perp}), \tag{S4}$$

where the factor of 2 for the $D_{\mathrm{v}}(\omega - \omega_{\parallel})$ accounts for the two-fold degeneracy of the in-plane vibrational mode. As shown in Fig. 4 b of the main text, the Ho out-of plane mode involves the motion of the oxygen atom underneath it, hence part of its amplitude is projected on the MgO phonon DOS. To account for this effect, in $D_{\mathrm{v}}(\omega - \omega_{\perp})$ we rescaled the peak amplitude to 0.4 to reproduce the relative heights of the phonon DOS peaks projected only on the Ho atoms, as calculated with DFT (see Fig. 4a of the main text). We then compute the related phonon energy density:

$$\rho_{\mathrm{Ho}}(\omega, T) = D_{\mathrm{Ho}}(\omega)\langle\hbar\omega\rangle = D_{\mathrm{Ho}}(\omega)\left[\exp\left(\frac{\hbar\omega}{k_{\mathrm{B}}T}\right) - 1\right]^{-1} \tag{S5}$$

to evaluate the transition probability obtained from the two-phonon integral [8, 23]

$$\Gamma(B, T) = \kappa\int_0^{\omega_c} \rho_{\mathrm{Ho}}(\omega, T)\rho_{\mathrm{Ho}}(\omega + \frac{\Delta}{\hbar}, T)\exp\frac{\hbar\omega + \Delta}{k_{\mathrm{B}}T}d\omega. \tag{S6}$$

Here, ω and $\omega + \frac{\Delta}{\hbar}$ are the frequencies of the two phonons involved in the transition, with $\Delta = 2\mu_{\mathrm{Ho}}B$ being the Zeeman splitting between the two lowest states with $\mu_{\mathrm{Ho}} = 10.1\,\mu_{\mathrm{B}}$ [20]. We set the cut-off frequency of the integration $\omega_c = E_c/\hbar = 100$ meV$/\hbar$ while κ is an overall scaling factor that depends on the properties of the materials and on the spin-phonon coupling [8]. Due to the peculiar single-bond-coordination of Ho atoms on MgO, most of the physical quantities used to determine this factor, such as the velocity of sound and material density, do not have a proper definition for the present system. Assuming a constant energy and momentum dependence of the spin-phonon coupling for the sake simplicity, the value of κ is, therefore, a constant, which is taken as a free parameter of the model. A more complete approach to compute the relaxation rate of single atom magnets by properly summing over all the momentum-dependent relaxation paths is beyond the scope of the present analysis and will be addressed in a future work.

The terms $\rho(\omega, T)$ and $\rho(\omega + \Delta/\hbar, T)\exp\frac{\hbar\omega+\Delta}{k_{\mathrm{B}}T}$ describe the absorption and emission of a phonon, respectively, connecting the two states separated by an energy $\Delta = 2\mu_{\mathrm{Ho}}B$, with $\mu_{\mathrm{Ho}} = 10.1\mu_{\mathrm{B}}$ [20]. The magnetic lifetime is obtained including the rates of the two possible reversal events ($|+\rangle$ to $|-\rangle$ and back) from the inverse sum of the respective rates, which can be expressed by [23]:

$$\tau_{\mathrm{s}}(B,T)^{-1} = \Gamma(B,T)\left[1 + \exp\frac{-\Delta}{k_{\mathrm{B}}T}\right]. \tag{S7}$$

Finally, the experimental lifetime is modeled by inversely adding the photon-limited lifetime τ_ν from the cascade of secondary electrons generated in the x-ray absorption process to the spin reversal lifetime:

$$\tau(B,T)^{-1} = \tau_\nu^{-1} + \tau_s(B,T)^{-1}, \tag{S8}$$

with the values of τ_ν taken from previous flux-dependent lifetime measurements [4]. In agreement with the analytical derivation presented in the work from D. L. Mills et al., the presence of a sharp resonance in the phonon DOS produces an exponential term in the temperature behavior of the spin relaxation [23]. As seen from the full curves in Figs. 2 and 3 of main text, our model reproduces the temperature- and field-dependent data for $\kappa = 1.7\times10^{-17}$, $\Delta E = 0.17$ meV.

To verify the potential role of delocalized MgO phonons to the reversal of Ho spins, we produce comparative models that include 2D delocalized phonons either in the absence or in the presence of local vibrational modes in the effective total DOS. According to our DFT calculations, the low-energy part of the MgO phonon DOS shows an almost linear increase with energy (see Fig. 4 of main text and first part of the blue curve of Fig. S3 above). Therefore, we firstly model the delocalized MgO phonons by a linear density of states:

$$D_{\mathrm{MgO}}(\omega) = \beta\hbar\omega, \tag{S9}$$

with a slope $\beta = 0.066$ meV^{-2} matching the DOS of Fig. 4a of the main text, and use the corresponding phonon energy density $\rho_{\mathrm{2D}}(\omega, T) = D_{\mathrm{2D}}(\omega)\langle\hbar\omega\rangle$ to compute the magnetic lifetime. Figure S4(a) shows the calculated temperature dependence of τ for low and high fields. The low field curve from our model follows closely the T^{-5} power law expected for Raman relaxation from phonons with 2D dispersion. Instead, the high field curve does not follow the same functional dependence and the calculated magnetic lifetimes are always lower than the corresponding low field values. This effects is generally valid for every monotonic phonon DOS and stems from the increased availability of phonons state for emission when larger splitting of the states are involved [8]. Figure S4(b) shows the comparison between experiments and calculated lifetime including the Raman process from delocalized phonon modes only and photon-induced relaxation background. As also discussed in Sec. II, this model provides a poor fit at low field and cannot capture at all the experimental behavior at high field.

We additionally test a comparative model that includes both delocalized and local vibrational modes. In this case, the total phonon density of states

$$D_{\mathrm{tot}}(\omega) = D_{\mathrm{MgO}}(\omega) + 2D_{\mathrm{v}}(\omega - \omega_{\parallel}) + D_{\mathrm{v}}(\omega - \omega_{\perp}) \tag{S10}$$

is computed by summing the amplitudes of all Ho- and MgO-projected components of the respective phonon DOS. Therefore, the total DOS at the in-plane and out-of-plane modes energy must follow the related degeneracy, namely 2 and 1, respectively. For this reason, we omit the rescaling factor of 0.4 for the out-of-plane peak at 8.6 meV (see Fig. 4a of the main text). We again use the phonon energy density $\rho_{\mathrm{tot}}(\omega, T) = D_{\mathrm{tot}}(\omega)\langle\hbar\omega\rangle$ to compute the magnetic lifetime as described above.

Figure S5 shows the result of the fit of temperature-dependent data with the relaxation model obtained using D_{tot} from Eq. S10, $\kappa = 1.0\times10^{-17}$, $\Delta E = 0.17$ meV. Although the low field data in Fig. S5a and low temperature data in Fig. S5b are quite well reproduced, the lifetime at high-field and high temperature cannot be captured by this model. This discrepancy is due to the overestimation of the coupling term between the spin and the delocalized phonon DOS. As the phonon DOS increases with the energy of the mode (see Eq. S9), more phonons are available to match the

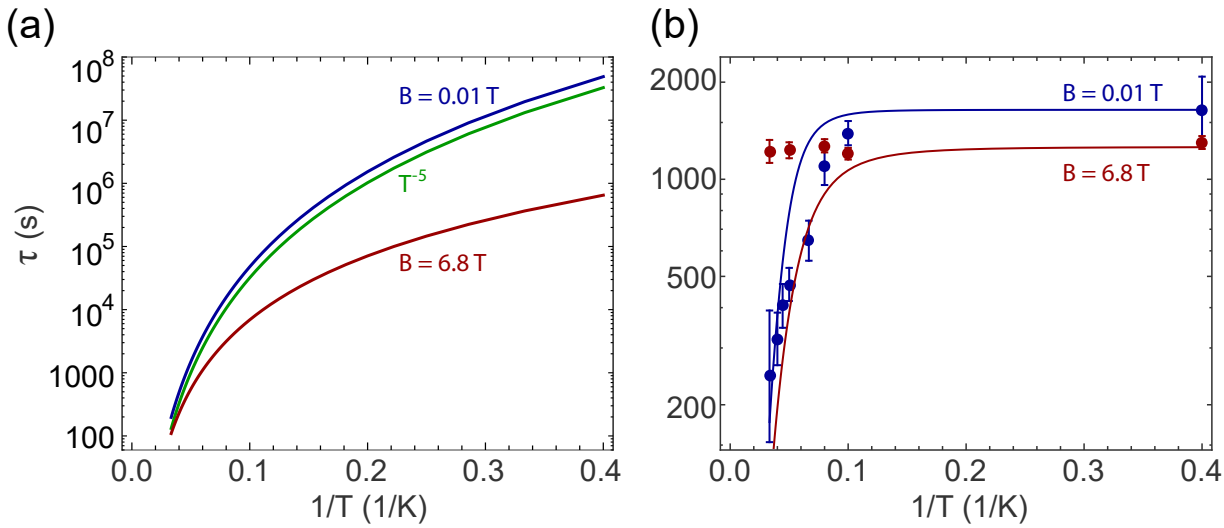

Figure S4. (a) Calculated magnetic lifetime, τ, for a two-phonon Raman process activated by delocalized MgO phonons with 2D dispersion (Eq. S9). Values obtained for $B = 0.01$ T (blue) and $B = 6.8$ T (red) are compared to a AT^{-5} power law (green) ($\kappa = 1.2 \times 10^{-16}$, $\mu_{\rm Ho} = 10.1\mu_{\rm B}$, $A = 3.5 \times 10^9$ sK^{-5}). (b) Magnetic lifetime, τ, as a function of temperature for $B = 0.01$ T (blue) and $B = 6.8$ T (red). Calculated magnetic relaxation τ including two-phonon Raman process with MgO phonons and photon-induced relaxation background (solid lines) are compared with experimental data (dots).

transition energies when the spin states are split in an external magnetic field. As a consequence, the contribution of the substrate phonons to the integral in Eq. (S6) increases with increasing values of $\Delta \propto B$. Using the model that only includes local displacements on the Ho atoms, the fits to high- field and high-temperature data are notably improved as shown in the main text in Fig. 2. These results suggest that the mechanism for Ho spin relaxation is predominantly the coupling with the local vibrational modes, as also proposed for molecular magnets [24]. As these modes induce a large Ho displacement with respect to the MgO lattice, they generate large low-symmetry distortions of the C_{4v} static crystal field of the oxygen top adsorption [4, 5], providing an efficient pathway to the spin relaxation [8].

Finally, we note that the localized vibrations provide significant contribution only to the two-phonon Raman processes, while no signature of direct process relaxation has been detected, i.e., at fields for which the Zeeman splitting matches the energy of the local modes (4.1 T and 7.4 T for the in-plane and out-of-plane mode, respectively).

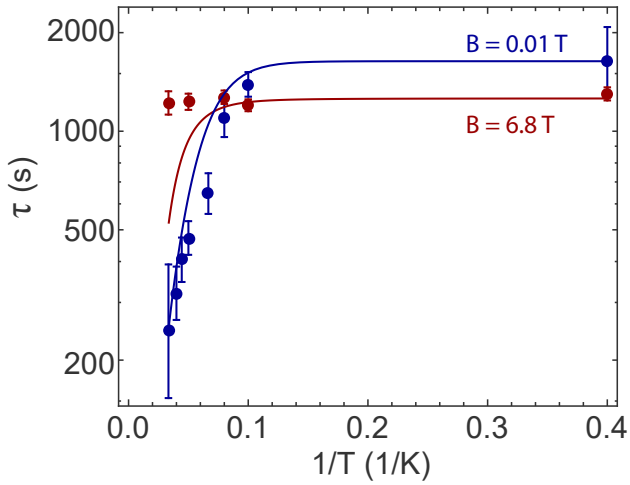

Figure S5. Magnetic lifetime, τ, as a function of temperature for $B = 0.01$ T (blue) and $B = 6.8$ T (red). Two-phonon Raman process including both Ho localized vibrations and delocalized MgO phonons contribution are shown as full lines ($\kappa = 1.0 \times 10^{-17}$, $\Delta E = 0.17$ meV, $\hbar\omega_{\parallel} = 4.7$ meV, $\hbar\omega_{\perp} = 8.6$ meV $\mu_{\rm Ho} = 10.1\mu_{\rm B}$) in comparison with experimental data shown as dots.

This suggests that the corresponding matrix element for transition of direct processes is significantly smaller than that of the Raman process.

V. ORBACH MODEL OF MAGNETIC RELAXATION

We test the validity of our conclusion by comparing these results with those obtained from a relaxation model that assumes only delocalized MgO phonons with 2D dispersion and a singlet excited state at $\overline{E} = \hbar\overline{\omega} = 4.5$ meV, as inferred from previous multiplet calculations [4]. In this case, an Orbach process with activation barrier $\overline{E}$ is expected to give a characteristic lifetime with an exponential temperature behavior, even in the absence of a localized mode [8]. The magnetization reversal rate for a two-phonon Orbach process is:

$$\overline{\Gamma}_{-J_z\to+J_z}(B,T) = \kappa^* \rho_{MgO}(\overline{\omega} - \frac{\Delta}{2\hbar}, T)\rho_{MgO}(\overline{\omega} + \frac{\Delta}{2\hbar}, T) \exp\frac{\hbar\overline{\omega} + \Delta/2}{k_{\mathrm{B}}T}, \tag{S11}$$

with

$$\rho_{MgO}(\omega, T) = D_{MgO}(\omega)\frac{\hbar\omega}{\exp\frac{\hbar\omega}{k_{\mathrm{B}}T} - 1} \tag{S12}$$

being the energy density of the MgO phonons only. Similarly to our analysis of the Raman process, we fit the experimental data by considering reversal from both J_z states and including the effect of the x-ray induced secondary electrons, as described in Eqs. (S7) and (S8). The results of the model for the temperature-dependent data at fixed field are shown in Fig. S6 for $\kappa^* = 5.0 \times 10^{-3}$ s^{-1}. Again, the low-field behavior is quite well reproduced, however, the model fails at high field. This failure is due to the decreasing separation between one of the Zeeman-split states of the lowest doublet and the excited-state singlet with increasing field, which produces a reduction of the energy barrier for reversal. The comparison between data and model indicates that long magnetic lifetimes at high magnetic field are not compatible with the presence of a first excited-state singlet at low energy. The presence of this singlet state, although predicted by multiplet calculations, has so far not been found in STM experiments [19, 20]. Our results further support the level schemes such as those discussed in Ref. [19] for explaining the magnetic states of Ho atoms.

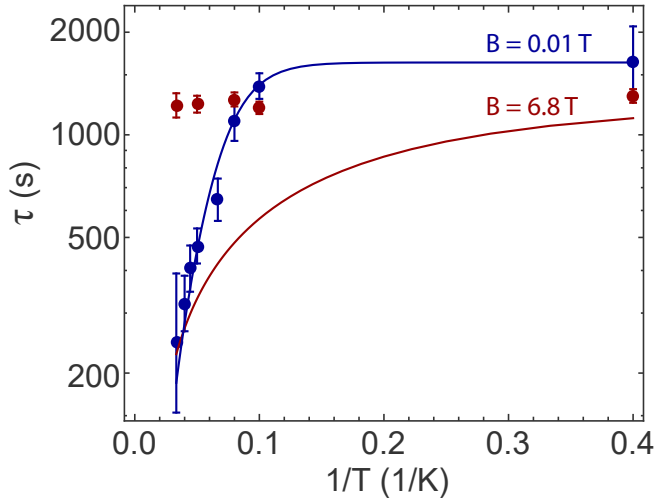

Figure S6. Magnetic lifetime, τ, as a function of temperature for $B = 0.01$ T (blue) and $B = 6.8$ T (red). Calculated τ including photon-induced relaxation background and a two-phonon Orbach process activated by delocalized MgO phonons with 2D dispersion (solid lines) are compared with experimental data (dots) ($\kappa^* = 200$, $\mu_{\mathrm{Ho}} = 10.1\mu_{\mathrm{B}}$, $\hbar\overline{\omega} = 4.5$ meV) in comparison with experiment shown as dots.

[1] C. Piamonteze, U. Flechsig, S. Rusponi, J. Dreiser, J. Heidler, M. Schmidt, R. Wetter, M. Calvi, T. Schmidt, H. Pruchova, J. Krempasky, C. Quitmann, H. Brune, and F. Nolting, J. Synchr. Rad. **19**, 661 (2012).

[2] K. Kummer, A. Fondacaro, E. Jimenez, E. Vélez-Fort, A. Amorese, M. Aspbury, F. Yakhou-Harris, P. van der Linden, and N. B. Brookes, J. Synchr. Rad. **23**, 464 (2016).
[3] J. Dreiser, R. Westerström, C. Piamonteze, F. Nolting, S. Rusponi, H. Brune, S. Yang, A. Popov, L. Dunsch, and T. Greber, Appl. Phys. Lett. **105**, 032411 (2014).
[4] F. Donati, S. Rusponi, S. Stepanow, C. Wäckerlin, A. Singha, L. Persichetti, R. Baltic, K. Diller, F. Patthey, E. Fernandes, J. Dreiser, Ž. Šljivančanin, K. Kummer, C. Nistor, P. Gambardella, and H. Brune, Science **352**, 318 (2016).
[5] E. Fernandes, F. Donati, F. m. c. Patthey, S. Stavrić, i. c. v. Šljivančanin, and H. Brune, Phys. Rev. B **96**, 045419 (2017).
[6] F. Donati, A. Singha, S. Stepanow, C. Wäckerlin, J. Dreiser, P. Gambardella, S. Rusponi, and H. Brune, Phys. Rev. Lett. **113**, 237201 (2014).
[7] A. Singha, F. Donati, C. Wäckerlin, R. Baltic, J. Dreiser, M. Pivetta, S. Rusponi, and H. Brune, Nano Lett. **16**, 3475 (2016).
[8] A. Abragam and B. Bleaney, *Electron paramagnetic resonance of transition ions* (Clarendon Press, Oxford, 1970).
[9] L. T. A. Ho and L. F. Chibotaru, Phys. Rev. B **97**, 024427 (2018).
[10] C. A. P. Goodwin, F. Ortu, D. Reta, N. F. Chilton, and D. P. Mills, Nature **548**, 439 (2017).
[11] F.-S. Guo, B. M. Day, Y.-C. Chen, M.-L. Tong, A. Mansikkamaki, and R. A. Layfield, Science **362**, 1400 (2018).
[12] G. Kresse and J. Furthmüller, Comput. Mat. Sci. **6**, 15 (1996).
[13] G. Kresse and J. Furthmüller, Phys. Rev. B **54**, 11169 (1996).
[14] A. Togo and I. Tanaka, Scr. Mater. **108**, 1 (2015).
[15] J. Perdew, A. Ruzsinszky, G. Csonka, O. Vydrov, G. Scuseria, L. Constantin, X. Zhou, and K. Burke, Phys. Rev. Lett. **100**, 136406 (2008).
[16] G. I. Csonka, J. P. Perdew, A. Ruzsinszky, P. H. T. Philipsen, S. Lebègue, J. Paier, O. A. Vydrov, and J. G. Ángyán, Phys. Rev. B **79**, 155107 (2009).
[17] K. Momma and F. Izumi, J. Appl. Crystallogr. **44**, 1272 (2011).
[18] L. Escalera-Moreno, J. J. Baldoví, A. Gaita-Ariño, and E. Coronado, Chem. Sci. **9**, 3265 (2018).
[19] F. D. Natterer, F. Donati, F. Patthey, and H. Brune, Phys. Rev. Lett. **121**, 027201 (2018).
[20] F. D. Natterer, K. Yang, W. Paul, P. Willke, T. Choi, T. Greber, A. J. Heinrich, and C. P. Lutz, Nature **543**, 226 (2017).
[21] P. R. Forrester, F. m. c. Patthey, E. Fernandes, D. P. Sblendorio, H. Brune, and F. D. Natterer, Phys. Rev. B **100**, 180405 (2019).
[22] C. Calero, E. M. Chudnovsky, and D. A. Garanin, Phys. Rev. B **74**, 094428 (2006).
[23] D. L. Mills, Phys. Rev. **146**, 336 (1966).
[24] S. Roychoudhury and S. Sanvito, Phys. Rev. B **98**, 125204 (2018).